Nuclear Materials and Energy 25 (2020) 100808

Contents lists available at ScienceDirect

Nuclear Materials and Energy

journal homepage: www.elsevier.com/locate/nme

Effects of a nitrogen seeded plasma on nanostructured tungsten films having fusion-relevant features

Andrea Uccello [a,*], Francesco Ghezzi [a], Laura Laguardia [a], Roberto Caniello [b], David Dellasega [a,c], Fabio dell'Era [a], Davide Della Torre [d], Riccardo Donnini [d], Gustavo Granucci [a], Ernesto Mesto [e], Daniele Minelli [a], Matteo Passoni [a,c], Matteo Pedroni [a], Andrea Pezzoli [c], Daria Ricci [a]

[a] Istituto per la Scienza e Tecnologia dei Plasmi, CNR, Via Cozzi 53, 20125 Milan, Italy
[b] Istituto di Fisica del Plasma "Piero Caldirola", Consiglio Nazionale delle Ricerche, IFP-CNR, Via Cozzi 53, 20125 Milan, Italy
[c] Dipartimento di Energia, Politecnico di Milano, Via Ponzio 34/3, 20133 Milan, Italy
[d] Istituto di Chimica della Materia Condensata e di Tecnologie per l'Energia, CNR, via Cozzi 53, 20125 Milan, Italy
[e] Dipartimento di Scienze della Terra e Geoambientali, Università degli Studi di Bari, "Aldo Moro", Via E. Orabona 4, 70125 Bari, Italy

ARTICLE INFO

Keywords:
Linear plasma device
GyM
Nitrogen seeded deuterium plasma
Tungsten coatings
Plasma facing components
Tokamak

ABSTRACT

Nitrogen (N) seeding is routinely applied in tokamaks with tungsten (W) walls to control the power exhaust toward the divertor. Open questions, concerning the interaction of N with W, are the influence of ion energy and W temperature on retention of implanted N and the erosion by deuterium (D) of the tungsten nitride being formed. Moreover, the extremely high particle fluxes in ITER and DEMO will erode the W tiles and the sputtered atoms will re-deposit forming W-based layers with a different behaviour toward the interaction with N seeded D plasmas.

In this work, W films with different morphology and structure were exposed to the N seeded D plasma of the linear device GyM, in order to address all these issues. The experiments were performed at the fixed N_2/D_2 partial pressure ratio of ~4% keeping the total pressure constant at 5.3×10^{-4} mbar. The exposure conditions were: (i) sample temperature of ~850 K, (ii) particle fluxes of $2-2.2\times10^{20}$ ions·m^{-2}·s^{-1} and (iii) particle energies up to ~320 eV. W columnar films (c-W) with properties close to those of virgin W coatings deposited on the tiles of JET Iter-Like Wall and ASDEX Upgrade and W amorphous films (a-W) resembling nanostructured W-based deposits found in present-day tokamaks and expected in ITER and DEMO, were considered. W columnar and amorphous coatings were produced by means of magnetron sputtering and pulsed laser deposition, respectively. The specimens were characterised by profilometry, X-ray depth-profiling photoelectron spectroscopy, optical microscopy, scanning electron microscopy, atomic force microscopy and X-ray diffraction. The main evidence is that the behaviour of the W films upon D+N plasma exposure in GyM strictly depends on their morphology and nanostructure. For all the films, a surface N-enriched layer, which is thermally stable and does not decompose at least up to ~850 K, is observed. Moreover, blisters are not present on the surface of the samples. The c-W coatings erode faster than the a-W ones and have a higher nitrogen retention and diffusivity. The mechanisms behind these results are here discussed together with their possible implications from the point of view of the topic of plasma–wall interaction in tokamaks.

1. Introduction

Seed of impurities into the edge plasma of full-metal tokamaks, like ASDEX Upgrade (AUG), JET Iter-Like Wall (JET-ILW) and ITER, is mandatory to lower the power flux to the outer divertor targets [1]. Recent experiments have shown that nitrogen (N) could be a good candidate as a seeding element since it keeps the radiation low in the plasma core, it efficiently cools the edge plasma and it also increases the plasma confinement [2]. The addition of N as an extra plasma species further complicates the plasma-first wall interaction issue [3]. This is particularly relevant for tungsten (W) based components, since nitrogen, unlike hydrogen and noble gases, can be significantly retained forming tungsten nitrides with lower melting temperature and higher sublimation rate [4]. Laboratory research activities have been devoted to the study of the interaction of: N plasmas [4,5] and N seeded deuterium plasmas (labelled with "D+N plasmas" in the following) [5–9]

* Corresponding author.
E-mail address: andrea.uccello@istp.cnr.it (A. Uccello).

https://doi.org/10.1016/j.nme.2020.100808
Received 5 August 2020; Received in revised form 7 October 2020; Accepted 9 October 2020
Available online 21 October 2020

with W surfaces, deuterium (D) plasmas with both W samples pre-implanted with N [10] and W_xN layers [5,11–13]. Most of the literature focuses on bulk W. Little attention has been paid to the behaviour of W films installed on some of the tiles in JET-ILW and AUG [14]. Even less attention has been given to the behaviour of W-based deposits found in present-day tokamaks, and expected in future fusion reactors like ITER and DEMO, after plasma sputtering of the first wall [15–19]. In general, W coatings can have very different properties with respect to those of the pristine tungsten. The investigation of the effects of a D+N plasma on W films is therefore really important.

In the present contribution, we describe the results of the exposures of different nanostructured W films to a D+N plasma of the linear machine GyM [20–22] at particle fluxes ($2-2.2\times10^{20}$ ions s^{-1} m^{-2}) and energies (up to ~320 eV) relevant to the main chamber of ITER [23] and the recessed regions of DEMO first wall [24]. In order to study possible thermal effects, the temperature of the samples was kept constant at the high value of ~850 K.

The aim of this work is to evaluate the erosion, the N retention and the compositional, morphological and structural modifications of the W coatings induced by the D+N plasma. We considered: (i) W columnar films which can simulate the virgin W coatings deposited on the tiles installed in JET-ILW and AUG [14] and (ii) W amorphous films resembling, in terms of morphology and structure, some of the nanostructured W-based deposits found in present-day tokamaks and expected in ITER and DEMO [15,16,18,25].

W films preparation and features, parameters of the exposures and details of the characterisation techniques are described in Section 2. The results of the exposures and their interpretation are presented in Sections 3 and 4 . Concluding remarks are given in Section 5.

2. Methods

Two types of W film with very different morphology and structure were prepared by magnetron sputtering (MS) and pulsed laser deposition (PLD), respectively. The MS W coatings mimic the films of the W-coated tiles of JET-ILW and AUG [14] and were produced at IPP-Garching. They had the typical columnar morphology of magnetron sputtered films with a mean crystallite dimension of ~20 nm. Their density is ~90% of that of bulk tungsten [26,27]. The PLD W films have morphology and structure resembling those of some of the W-based deposits retrieved from the present-day tokamaks and expected in ITER and DEMO [15,16,18,25]. They were deposited at NanoLab of Politecnico di Milano. They showed an amorphous-like compact featureless morphology with no long range order and a mean crystallite dimension of ~1 nm. The density of these coatings is ~11.5 g/cm^3. The details of the deposition conditions are given in [28] and [29,30] for the MS and PLD W films. In the following, the MS columnar and the PLD amorphous-like coatings are labelled with c-W and a-W, respectively. All the films had a mean thickness of 300 nm and were deposited on 1 × 1 cm^2 silicon, Si(100), substrates. Their root mean square (RMS) roughness is on the order of few nanometres.

W coatings were exposed to a N seeded D plasma in the steady-state linear plasma machine GyM (Fig. 1a and b) [9,12,20–22,27,31]. The exposures were performed at the fixed N_2/D_2 partial pressure ratio of ~4% keeping the total pressure constant at 5.3×10^{-4} mbar (GyM base pressure is $\sim10^{-7}$ mbar). The axial magnetic field was ~80 mT in the sample exposure region. Plasma was generated by a 2.45 GHz microwave (MW) source delivering a power of 1.2 kW. A Langmuir probe (single stainless steel probe tip of 0.75 mm in radius and 10 mm in length) was used to evaluate the plasma density n_e, electron temperature T_e, plasma potential V_p and ion flux Φ_i. The probe was kept at 6 cm from the machine axis. Since the radial profiles of the plasma parameters of GyM are nearly constant within a radius of 10 cm [21], the estimated values are also representative of those at the plasma centre. Under these conditions, $n_e = 3.5 - 4.0\times10^{16}$ m^{-3}, $T_e = 3.5 - 4$ eV, V_p ~21 V and $\Phi_i = 2 - 2.2\times10^{20}$ ions·s^{-1}·m^{-2} were obtained.

A stainless steel (SS) manipulator with a heatable and biasable SS sample holder was used for the exposures (Fig. 1c) [27]. A negative bias voltage is applied to attract ions only to the sample holder which is electrically insulated from the grounded manipulator by an alumina ring. Maximum negative bias voltage and exposure temperature are −400 V and ~850 K. The temperature of the samples was measured by a thermocouple placed within the manipulator and by a pyrometer. Since the line-of-sight (LoS) of the pyrometer is normal to the GyM axis, exposures were done at an angle of 45° between the sample holder normal and the pyrometer LoS. The sample holder can accommodate up to four 1 × 1 cm^2 samples (Fig. 1d). For each exposure, two c-W and two a-W films were loaded. One of each was half masked with a molybdenum (Mo) foil in order to measure the eroded step by a mechanical profilometer at the end of the experiment, and to separate the thermal effects on the coatings from those of the plasma exposure. The unmasked samples were also needed to ease some of the other characterisation techniques (see below).

Two exposures of the c-W and a-W films to the D+N plasma of GyM up to a fluence of some 10^{24} ions·m^{-2} at a temperature of ~850 K were done at the two different sample holder bias voltages of −100 V and −300 V. The exposure at −100 V lasted 4 h. The exposure at −300 V was interrupted after 3 h, due to technical limitations. The samples were heated at ~850 K before the plasma exposure and then the temperature was kept constant by means of a proportional–integrative–derivative PID controller which used the pyrometer temperature as the process variable. We chose −100 V and −300 V as bias voltages (which correspond to an ion energy of ~120 eV and ~320 eV, taking V_p into account) in order to be well below and above the W sputtering threshold (E_{th}) for D^+ ions (which is ~200 eV [28,32]). Erosion of the films was expected also for the lower bias voltage due to N^+ ions for whom E_{th} is between 60–70 eV [33]. Together with D and N atomic and molecular ions, the impurities present in the plasma could contribute to some extent to sputtering. Starting with oxygen (O) and carbon (C) impurities, they could come from the grounded wall of GyM as a consequence of the physical desorption of adventitious carbon and the thermal desorption of water. The biased stainless steel sample holder was another source of oxygen and carbon, mainly in the form of sputtered O and C atoms. Considering heavy impurities, iron (Fe) atoms could be also sputtered from the sample holder. Molybdenum atoms could be eroded from the Mo mask (for profilometry) which was biased too. All these light and heavy neutral impurities needed to be ionised in order to effectively sputter the W films. However, due to the relatively low density of the plasma of GyM, the values of the mean free path (MFP) for the different ionisation reactions are of the same order of magnitude of or greater than the characteristic dimensions of the experiment, that are the diameter of 25 cm and the length of 2.11 m of the vacuum vessel of GyM (for example, the MFP for electron impact ionisation of a Mo atom is over 1 m). Neutral impurities coming from the wall and the sample holder had therefore a great chance to reach the wall of the machine or the sample holder before being ionised. For this reason, their contribution to the sputtering of the W films should have been low. In support of this, with regard to heavy impurities, the absence of Fe and Mo signals in the X-ray photoelectron spectroscopy (XPS) spectra of the exposed samples is a clear sign of the low level of implanted Fe and Mo atoms that might have led to a strong erosion of the samples.

c-W and a-W films were characterised before and after the exposures to study the possible different effects of the D+N plasma of GyM. The plasma erosion was evaluated by a KLA Tenchor mechanical profilometer, measuring the eroded step height between the exposed and the masked side of the films (twenty independent chords were taken at different positions and the average value and standard deviation of the step were calculated). Morphological changes of both the exposed and masked sides of the c-W and a-W films were studied by means of

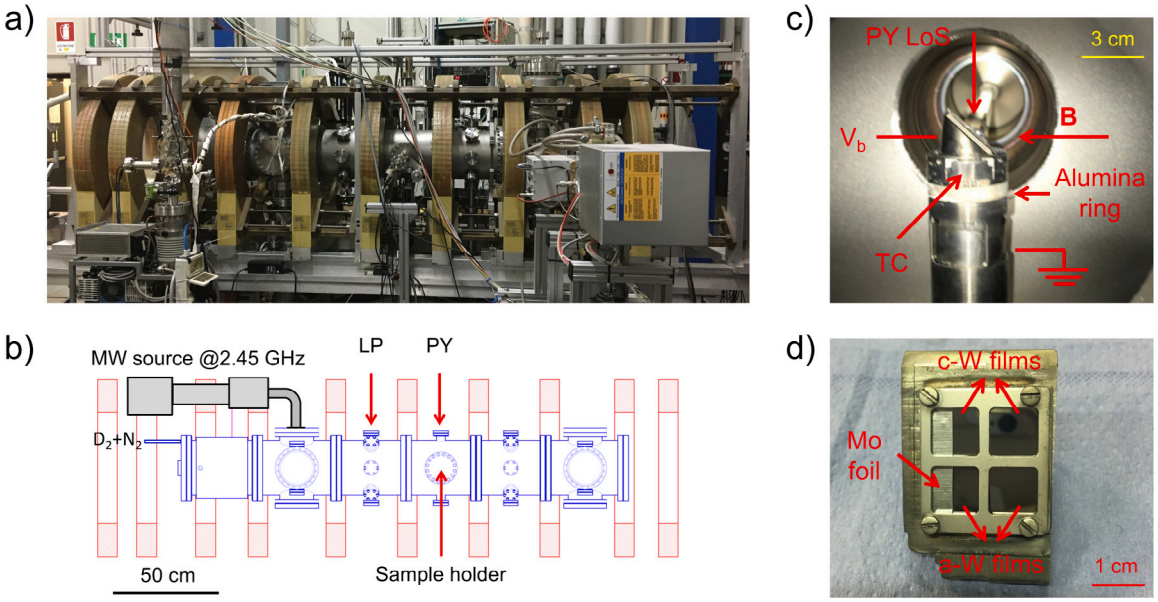

Fig. 1. (a) A photograph of the steady-state linear plasma machine GyM. (b) A scheme of GyM with the axial position of the Langmuir probe (LP), the pyrometer (PY) and the sample holder. (c) A photograph of the manipulator and the sample holder with the location of the thermocouple (TC) and the line-of-sight of the pyrometer (PY LoS). The biasable sample holder at bias voltage V_b is electrically insulated from the grounded manipulator by an alumina ring. (d) The arrangement of the two c-W and the two a-W samples into the holder. One c-W and one a-W film are half masked by a molybdenum (Mo) foil.

an optical microscope and a Zeiss Supra 40 field emission scanning electron microscope (SEM, accelerating voltage 3–6 kV). The topography of the samples was obtained by means of a NanoRTM Atomic Force Microscope (AFM) in air (Pacific Nanotechnology, Santa Clara, CA, USA). Measurements were done in contact mode at a scan speed of 0.5 μm s^{-1} with a scan size of 10 × 10 μm^2. Considering the unmasked samples, structural modifications were investigated with a Siemens D500 X-ray diffractometer (XRD) with Bragg–Brentano geometry and copper Kα radiation. The X-ray data were collected in the 2θ range 20°-90° with step size of 0.1° and velocity 5 s/step. Compositional changes of the surface and subsurface layers of the films were studied by a depth-profiling XPS system primarily consisted of a VSW CLASS 100 hemispherical analyser and a non-monochromatic aluminium Kα X-ray source [34]. Both survey and high-resolution XPS spectra, respectively with an overall instrumental resolution of ~2 eV and ~0.96 eV, were acquired for the W samples before and after the exposures at each ion gun sputtering time (see below). The XPS spectra of as-deposited and exposed samples showed W and N signals, together with those of C and O impurities. All the peaks of W4f, N1s, C1s and O1s lines were fitted. In particular, the tungsten W4f and carbon C1s lines were fitted with Doniach–Sunjic functions using asymmetry factors of 0.09 and 0.07. The fitting of nitrogen N1s and oxygen O1s lines was instead done through Voigt profiles, after a Shirley background subtraction. Relative atomic concentrations were finally evaluated by using atomic sensitivity factors experimentally determined from the Lindau's cross sections [35–37].

The XPS apparatus is also equipped with an impact ionisation ion gun VG EX05 for imaging and depth-profiling. XPS depth-profiling of the samples was done before and after the exposures using 3 keV Ar^+ ions at a current density of 3 μA cm^{-2}. The Ar^+ sputtering rate was determined measuring the depth of the crater done on a virgin c-W (with RMS roughness of few nm) using the mechanical profilometer. Aware of the shallow projected range of nitrogen ions (N^+) at the bias voltages of interest (up to 5 nm, as evaluated with TRIM [38], see Section 4), the depth profile was acquired sampling the subsurface more than the bulk. Specifically, the considered sputtered depths are: 3 nm, 4.5 nm, 7.5 nm, 10.5 nm, 13.5 nm, 16.5 nm. Since one of the goals of this work is to evaluate the N retention of the samples after the exposures, the depth profile of each exposed sample extends as long as the N1s signal was detected.

Table 1
Sample labels, exposure conditions and profilometry results. Since the fluence of the two exposures was different, the eroded step as well as the erosion rate (the ratio between the eroded step and the exposure time) are reported. NM stands for not measurable.

Sample	Bias [V]	Fluence [ions·m^{-2}]	Eroded step [nm]	Erosion rate [nm/s]
c-W	−100	$2.6{\cdot}10^{24}$	31 ± 9	$21.5{\cdot}10^{-4} \pm 6.3{\cdot}10^{-4}$
a-W	−100	$2.6{\cdot}10^{24}$	NM	NM
c-W	−300	$1.8{\cdot}10^{24}$	145 ± 23	$134.3{\cdot}10^{-4} \pm 21.3{\cdot}10^{-4}$
a-W	−300	$1.8{\cdot}10^{24}$	66 ± 10	$61.1{\cdot}10^{-4} \pm 9.3{\cdot}10^{-4}$

3. Results

The results of the profilometer measurements are reported in Table 1. Since the fluence of the exposures at the two bias voltages is different, the erosion rate (i.e. the ratio between the eroded step and the exposure time) is also given. It is clear that the magnetron sputtered c-W films were more easily eroded by the D+N plasma than the PLD a-W coatings. Considering the exposure at −100 V, the erosion of the a-W sample was below the profilometer depth resolution of some nanometres. The eroded step of the c-W specimen was instead measurable. The erosion rate of the c-W film increases six times from −100 V to −300 V. At −300 V the c-W coating was eroded twice the a-W film.

The effects of the exposures on the W films morphology were investigated by optical microscopy and SEM. Optical microscope images (not reported here) and SEM pictures show no evidence of blisters formation on the surface of c-W and a-W samples after the exposures to the D+N plasma of GyM. Fig. 2 displays the SEM top-view images of the surface of the c-W films (a–c) and a-W films (d–f) as deposited (a, d) and after D+N plasma exposure at −100 V (b, e) and at −300 V (c, f). In order to separate the thermal effects from those of the plasma interaction, two SEM images are shown for each exposed W film: the first is relative to the side under the molybdenum foil (masked, "M") and the second is relative to the unmasked side (exposed, "E"). For all the samples, a morphology change is evident after the two experiments and it is very different for the c-W and a-W films. Comparing the E-side of figures (b) and (e) with the E-side of figures (c) and (f), it is also clear that no dramatic morphology variation was obtained changing the bias voltage

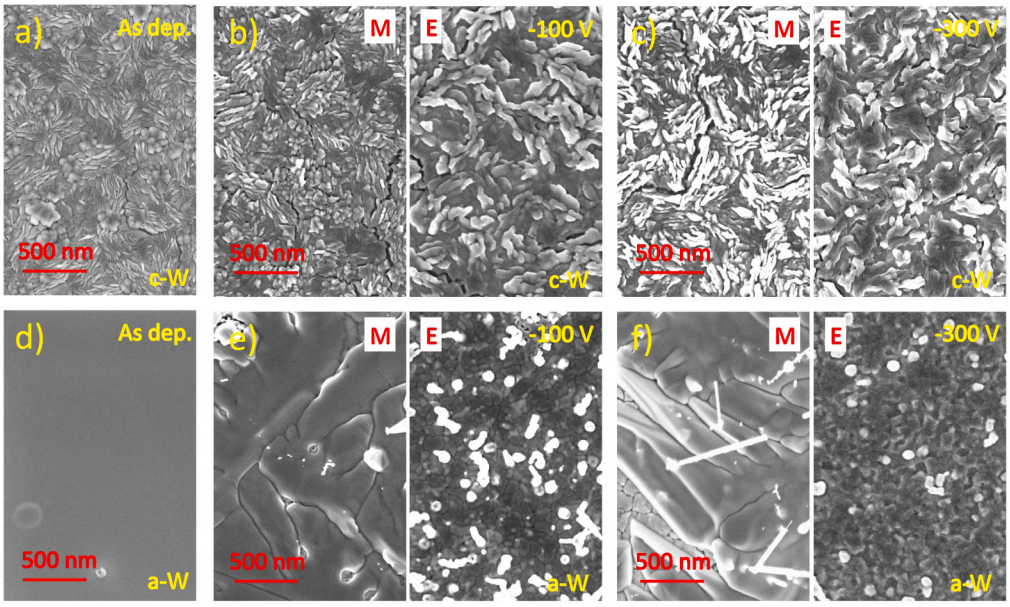

Fig. 2. SEM top-view images of the c-W as deposited (a) and exposed to the D+N plasma of GyM at −100 V (b) and at −300 V (c). SEM top-view images of the a-W as deposited (d) and exposed at −100 V (e) and at −300 V (f). For each exposed sample, two SEM micrographs are shown: one of the masked side under the molybdenum foil (labelled with "M") and one of the unmasked side (labelled with "E", exposed).

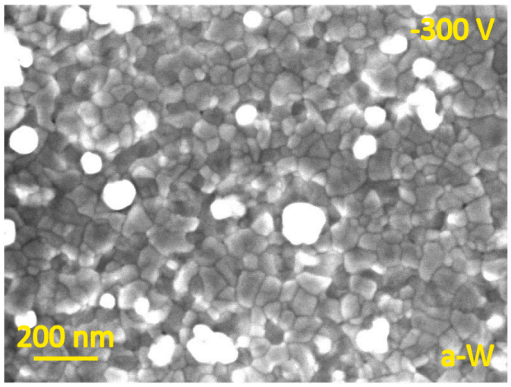

Fig. 3. Magnification of the E-side of the SEM image 2f relative to the a-W film exposed at −300 V to the D+N plasma of GyM.

and fluence. Considering the masked side of the c-W films, figures (b) and (c) are very similar to figure (a) of the as deposited sample suggesting that thermal effects on the c-W morphology are negligible. Therefore, it is possible to assume that the differences between the SEM micrographs of the E-side and that of the as deposited sample can only be ascribed to the interaction of the coating surface with the plasma. In particular, the E-side of figures (b) and (c) shows a growth of the grains that happened during the exposures. For the a-W films the situation is very different. The featureless surface of the as deposited sample of figure (d) is far from both the M and E-sides of figures (e) and (f). Moreover, for the two exposed a-W films, a relevant morphology change between the two sides is clear. Contrary to what was claimed for the c-W samples, thermal effects are thus really important for the a-W films [31]. From the E-side of figures (e) and (f), crystallisation and grain growth of the highly disordered amorphous-like W film structure can be appreciated. This is even more evident from the SEM image of Fig. 3 which depicts the surface of the E-side of the a-W film exposed at −300 V at a high magnification.

Fig. 4 shows the AFM topographies of the exposed samples. In order to evaluate the standardised one-dimensional roughness parameters, 9 line profiles along the scanning x axis (500 nm apart along the y direction) were considered for each AFM image. Each one-dimensional texture was split into waviness (the low-frequency components defining the overall shape) and roughness (the high-frequency components) at the cut-off frequency of 0.3 times the Nyquist frequency, i.e. 250 nm of real-space wavelength, using Gwyddion open source software [39]. For all the line profiles of each AFM image, the analysis of the peaks and valleys of the waviness was done and the results are shown in Table 2. The average of RMS roughnesses, R_q, of the 9 one-dimensional textures after the removal of the waviness is also reported. It is clear from the table that the surface texture of all the exposed samples is characterised by smooth peaks and valleys on the nanometre-scale, superimposed by a roughness having a RMS of 2 nm at most. This shallow profiling justifies the depth resolution of few nm that we claimed in Section 2 for the XPS depth-profiling measurements.

Table 2
Sample labels, exposure conditions and AFM results. h and w are the average height and width of the peaks and valleys of the 9 line profiles along the x axis examined for each AFM image. $\overline{R_q}$ is the average of RMS roughnesses associated to the 9 one-dimensional textures after the removal of the waviness.

Sample	Bias [V]	h [nm]	w [nm]	h/w	$\overline{R_q}$ [nm]
c-W	−100	22.5	81.6	0.28	1.4
a-W	−100	18.5	67.1	0.28	2.1
c-W	−300	29.9	96.5	0.31	1.4
a-W	−300	6.5	56.0	0.12	1.3

All the survey XPS spectra of c-W and a-W films before and after the exposures showed only the W, N, C and O signals at each sputtering time. The high-resolution spectra were thus acquired for W4f, N1s, C1s and O1s core levels. The values of the XPS peak shifts due to tungsten nitrides (WN_x) formation are quite scattered in literature [4,40–42]. Moreover, the overlap at the same binding energies (BEs) of other possible peaks associated to oxides and carbides makes the assignment of each feature of the XPS spectra to the correct chemical state extremely difficult. In the following, the most reasonable peak assignment of the measured XPS spectra is given, mainly based on the available literature and on the current knowledge of the authors.

Starting with the as deposited samples, Figs. 5 and 6 show the XPS data and fit results for the surface and the first subsurface layer (after 3 nm of sputtering) of the c-W and a-W films, respectively. The

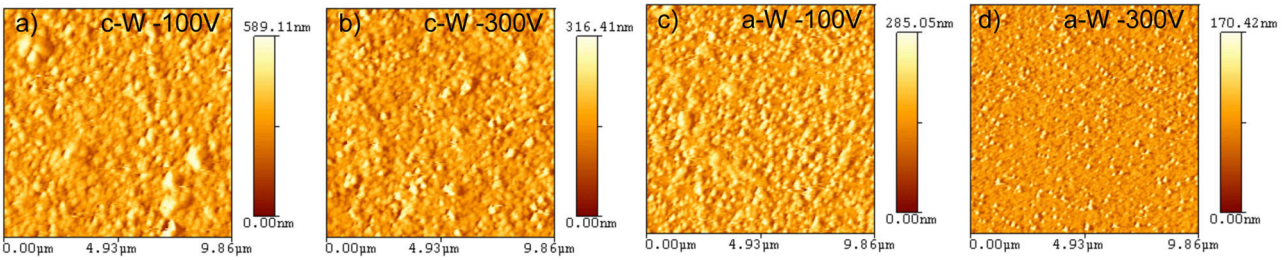

Fig. 4. AFM images of exposed a-W and c-W films at −100 V (a,c) and −300 V (b,d).

W4f core level of c-W film at the surface shows four components. We assign the doublet at 31.8 eV to metal W4f7/2 and the contributions at 32.6 eV, 35.7 eV and 36.4 eV to the tungsten oxides WO_2, non-stoichiometric WO_x and WO_3 (a fifth small component at 37 eV due to the contribution of the W5p3/2 state is also present in every W4f core level spectrum but it was not reported in the figures for the sake of clarity). Considering the O1s core line, the different tungsten oxides lead to the peaks at 530.6 eV, 531.3 eV and 532.3 eV, respectively. A contribution to the 531.3 eV peak comes also from the C-OH bond type. At about 532.3 eV and at 533.4 eV, the signals of inhomogeneous plasma polymerisation products (labelled with "A" and "B"), formed during the magnetron sputtering deposition because of the presence of carbon, oxygen and hydrogen in the vacuum chamber and in the weak plasma which surrounded the MS target, are located [43]. The corresponding peaks of C-OH, A and B under the C1s spectrum are located at 285.2 eV, 287.3 eV and 288.8 eV. The C1s core level shows also two contributions at 284.4 eV and 286.1 eV which we assign to C–C graphitic state and C-O bond type. The N1s spectrum shows three components at 400.5 eV, 401.7 eV and 402.7 eV. We suppose that these peaks are associated to some un-ordered W nitride phases formed during the final phases of the deposition process [44].

After 3 nm sputtering of the as deposited c-W film, the W4f core line shows only two components. We assign the doublet at 31.7 eV to an unresolved metal tungsten and surface tungsten carbide (WC_{surf}) component. We associate the doublet at 32.6 eV to the bulk signal of the carbide state (WC_{bulk}). The presence of tungsten carbide is also testified by the appearance of the two peaks at 281.5 eV and 283.2 eV under the C1s core line [43]. From both the W4f and O1s spectra it seems that, among the different tungsten oxides detected on the surface, only the WO_2 survives. Moreover, no N1s peak was observed.

Moving on to the as deposited a-W film (Fig. 6), the W4f and O1s core levels show the same contributions at the surface as the c-W film. The N1s peak was instead not detected. At the subsurface (i.e. after 3 nm of sputtering), the tungsten carbide surface and bulk signals are not present under the W4f and C1s core levels. From Figs. 5 and 6 and from the relative atomic concentrations of the as deposited c-W and a-W films reported in Fig. 8 we can infer that the a-W film has a higher content of tungsten oxides both at the surface and subsurface but it does not show any nitrogen contamination (and only trace of carbon contamination). The high percentage of oxygen is indeed a peculiar feature of the PLD W amorphous morphology [29]. O, C and N content of the c-W film was probably due to the contamination of the magnetron sputtering deposition process [28].

The interaction with the D+N plasma of GyM clearly led to a significant change of the chemistry of the surface layers of the W coatings. Since the different contributions to the XPS spectra of the samples exposed at the two bias voltages are almost the same, we limit to discuss the peak assignment for to the samples exposed at −100 V. The relative atomic concentrations are given instead for all the samples (see Fig. 8). Fig. 7 shows the W4f and N1s XPS data and fit results for the surface and the subsurface layers (up to 16.5 nm of sputtering) of the c-W (left column) and a-W (right column) samples exposed at −100 V. We decided to show only these two core levels because the fitting of the O1s and C1s core lines does not report components different from those we found for the as deposited films. Considering the W4f core level of the c-W film surface, the doublets at 31.6 eV and at 35.5 eV are again assigned to the metal W4f7/2 and to the WO_x states. The features at 32.3 eV and 36.4 eV are now associated to the unresolved WO_2+W_2N state (with a contribution from WC_{bulk} below the surface) and to the unresolved WO_3+WN metastable state. This assignment is supported by the fitting of the N1s core level. As a matter of fact, the nitrogen signal of the surface can be obtained from the sum of five contributions. The peaks at 397.9 eV and 399.6 eV are assigned to the W_2N and WN states, respectively. The peaks at 400.7 eV, 401.8 eV and 402.8 eV are associated to ND, ND_2 and ND_3 species, bound to W with a different number of coordination sites maintaining the valence of nitrogen constant. Evidence of these bondings was observed in case of transition metals used to synthesise ammonia [45–47]. While the ND_x peaks were detected only at the surface, the W_2N and WN contributions survive up to 16.5 nm. Moving on to the a-W sample surface, the doublets of metal W4f7/2 and WO_x states are at the same place of c-W film surface W4f spectrum. The component of the unresolved WO_2+W_2N state and that of the unresolved WO_3+WN metastable state are now located at 32.7 eV and 36.3 eV. With regard to the fitting of the N1s line, tungsten nitrides lead to the peaks at 397.6 eV and 399.9 eV assigned to W_2N state and unresolved ND+WN state (the low counting rate hampers the deconvolution of ND and WN contributions). Components at 401.2 eV and 402.3 eV are due to ND_2 and ND_3 species. The fitting of the C1s line shows that no carbides are present at the surface of the sample. The WC_{bulk} state was instead detected at 281.3 eV after 3 nm of sputtering and at 32.2 eV under the unresolved WO_2+WC_{bulk} state in the W4f core level spectrum. The latter consists also of the doublet of metal W4f7/2 at 31.4 eV. Nitrogen was not detected under the surface. From Fig. 8 of the relative atomic concentrations of the samples and from Fig. 9 which depicts the behaviour of the N1s peak area as a function of the sputtering depth for all the films, we can make some comments limited to the behaviour of W and N (which are the focus of this work). It is noted that the exposure at −100 V lasted 25% more than that at −300 V. (i) For the c-W films, nitrogen is detected also below the subsurface while it is only present at the surface of the a-W samples (N concentration at 3 nm and 4.5 nm depths for the a-W film exposed at −300 V is well below the XPS detection limit of 1%). (ii) For the c-W films, nitrogen is present deeper in the bulk after the exposure at −100 V; this is not true for the a-W samples. (iii) At the same depth, the N relative atomic concentration of c-W films is higher for the −100 V case than for the −300 V case. This picture is reversed for the a-W samples.

The structural changes of the films exposed to the D+N plasma of GyM were studied by XRD. Fig. 10 shows the XRD spectra of c-W (Fig. 10a) and a-W (Fig. 10b) films as deposited and after both the exposures at −100 V and −300 V. The detected peaks are those of the main crystallographic phase of bulk W, the α-phase (together with the strong Si(100) peak from the substrate, which was cut-off to improve the readability of the plots). Moreover, a small peak of W_2N(200) can be seen in the spectra of the exposed c-W films [48]. This evidence is consistent with the XPS results of Figs. 7 (left column), 8 and 9. Considering the as deposited c-W film (Fig. 10a), the structure is partly oriented along the α-W(110) direction. The slight reduction of the intensity of the α-W(110) peak in the XRD spectra of the exposed

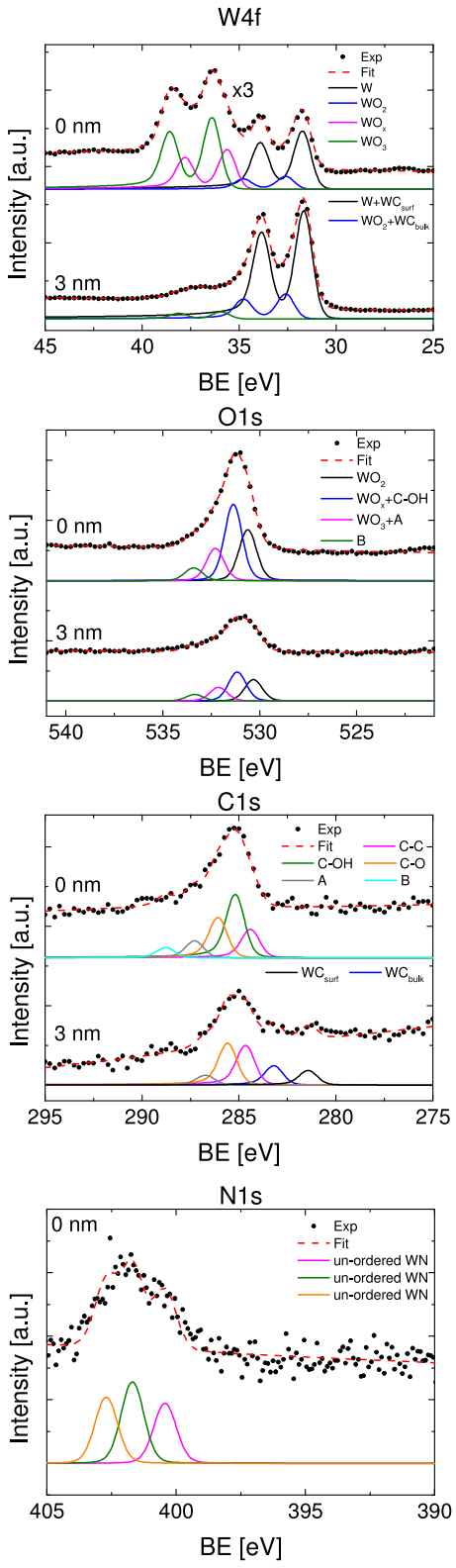

Fig. 5. From the top to the bottom: W4f, O1s, C1s and N1s core level XPS spectra of the surface and subsurface (after 3 nm of sputtering) of the c-W film as deposited. Filled circles: measured data; lines: mathematical fits. The solid lines are the fit components, the dashed line is the fit sum. (For interpretation of the references to colour in this figure legend, the reader is referred to the web version of this article.)

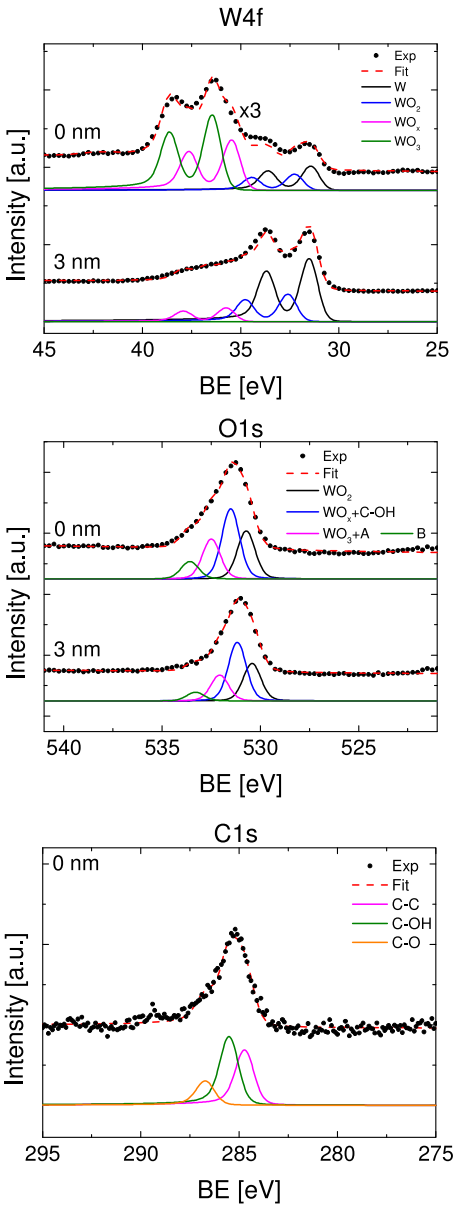

Fig. 6. From the top to the bottom: W4f, O1s and C1s core level XPS spectra of the surface and subsurface (after 3 nm of sputtering) of the a-W film as deposited. Filled circles: measured data; lines: mathematical fits. The solid lines are the fit components, the dashed line is the fit sum. (For interpretation of the references to colour in this figure legend, the reader is referred to the web version of this article.)

films is related to the loss of thickness due to the plasma erosion. Fitting the α-W(110) peak with a Lorentzian function and using the Scherrer's formula [49], it was possible to extrapolate the mean crystallite size (MCS) of the c-W films. The MCS of the as deposited sample is around 20 nm and increases to 27 nm and 34 nm for the samples exposed at −100 V and −300 V. These larger values of MCS can be ascribed to a slight defects recovery of the films which took place during the exposures, as a consequence of both the interaction with the plasma species and the high temperature of the samples. The increase of MCS is also corroborated by the SEM micrographs of the Fig. 2b and c relative to the E-side of the c-W films which show a small increase of the grain dimension.

The XRD spectrum at the diffraction angle corresponding to the α-W(110) direction of the as deposited a-W sample exhibits a broad band in place of the peak of the c-W samples (Fig. 10b). This is the typical feature of the highly disordered PLD amorphous-like W films [29]. The appearance of the α-W(110) peak after both the experiments is a

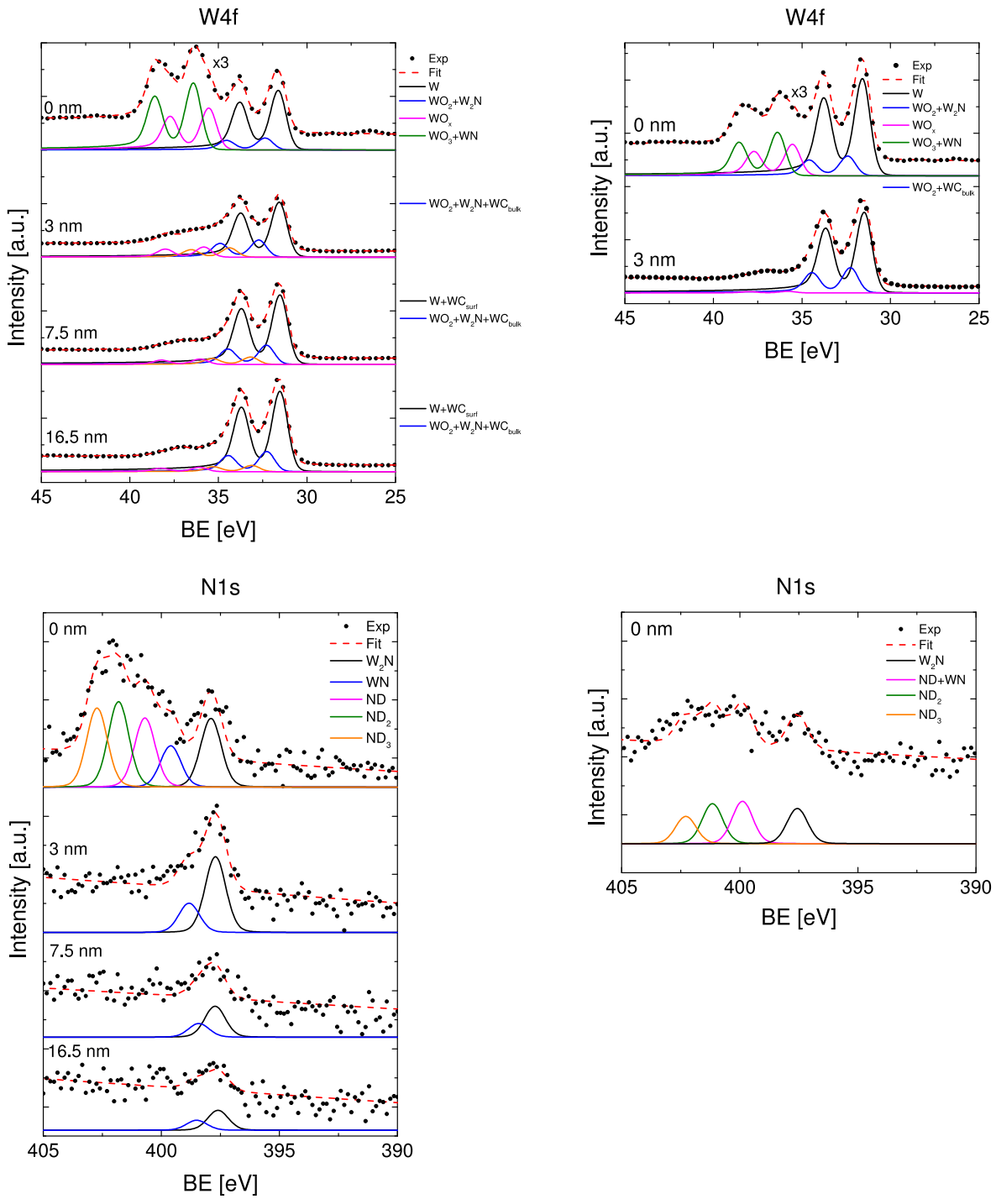

Fig. 7. W4f and N1s core level XPS spectra of the surface and subsurface layers of c-W (left) and a-W (right) films exposed in GyM at a bias voltage of −100 V. Filled circles: measured data; lines: mathematical fits. The solid lines are the fit components, the dashed line is the fit sum. (For interpretation of the references to colour in this figure legend, the reader is referred to the web version of this article.)

clear sign of a strong crystallisation of the a-W films. This confirms the interpretation of the SEM images of the E-side of Fig. 2e and f and of Fig. 3. Using the Scherrer's formula again, the MCS of the a-W film as deposited of ~1 nm becomes 35 nm and 37 nm for the exposed samples at −100 V and −300 V. Albeit these values of the MCS are close to those of the exposed c-W films, the shape of the grains is different. Unlike the columnar grains of the as-deposited MS film, which do not noticeably change during the exposures (see SEM image 2a and the E-side of SEM Fig. 2b and c), SEM images of the exposed a-W films (E-side of Fig. 2e and f and Fig. 3) show the growth of isotropic grains, whose dimension is of the same order of magnitude of the MCS. The crystallisation and grain growth of the a-W samples are mainly due to the recovery of point defects and dislocations and to the desorption of part of the oxygen present in the films after the deposition process [30].

4. Discussion

Section 3 clearly shows that the behaviour of W films under D+N plasma exposure at the high temperature of ~850 K for different bias voltages strictly depends on their morphology and nanostructure. First

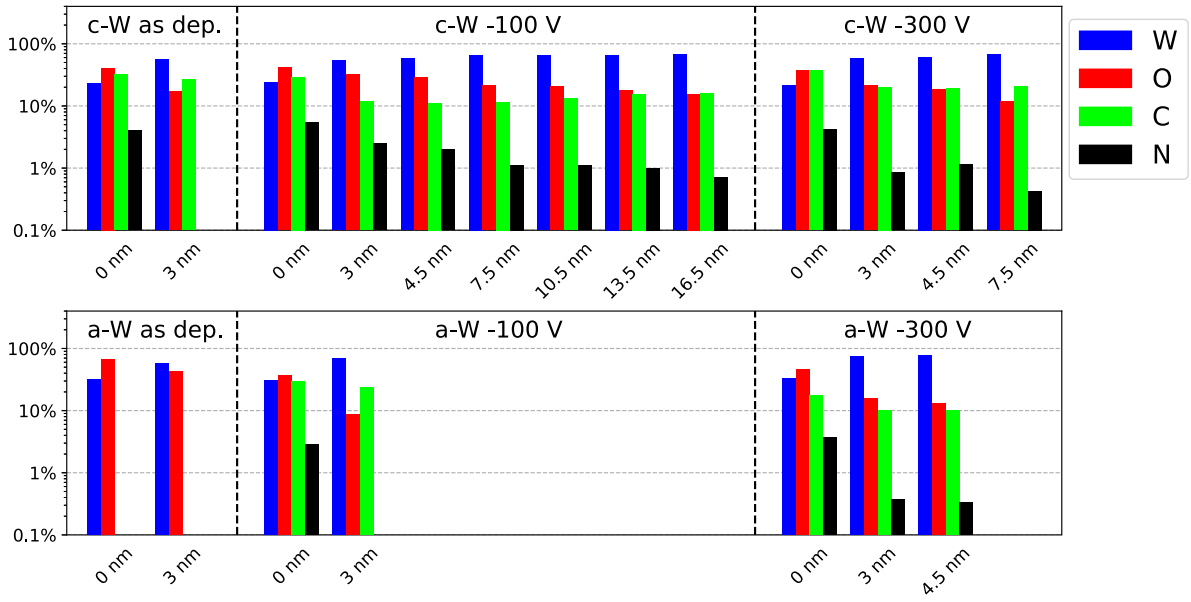

Fig. 8. Relative atomic concentrations of surface and subsurface layers of the c-W (first row) and a-W (second row) films before and after the exposures. The log-10 scale is used for the *y*-axis of the two plots to highlight the small values of nitrogen relative atomic concentration. (For interpretation of the references to colour in this figure legend, the reader is referred to the web version of this article.)

of all, the profilometry measurements (see Table 1) highlight that the erosion rate of c-W films is significantly higher than that of a-W layers, which is even not measurable for −100 V bias voltage. Since the sputtering threshold of the c-W films for D^+ is ∼200 eV [28], the erosion of the specimen exposed at −100 V (ion energy of ∼120 eV) can be entirely ascribed to the nitrogen seeding ions N^+ whose E_{th} was computed to be between 60 eV and 70 eV [33]. Sputtering of a-W film at −100 V by both deuterium and nitrogen ions was instead negligible. At -300 V (ion energy of ∼320 eV), the c-W film was also effectively sputtered by D^+ ions leading to a significant increase of the erosion rate which is however more than twice that of the a-W sample. The lower erosion rate of a-W films at the two bias voltages could be related to the properties of the W films. In particular, the peculiar morphology and nanostructure of c-W and a-W specimens reflect on their different density (see Section 2) and possibly on their surface binding energy, both of which significantly affect the sputtering yield. Considering the density (ρ), the modelling work with the code OKSANA described in [50] shows that the sputtering yield (Y) of light ions on heavier targets at a given ion energy increases with the density. This is consistent with the lower erosion rate of the less dense a-W films with respect to that of c-W films as evaluated from profilometer measurements for each bias voltage. However, the dependence of Y on ρ found by the authors of [50] is rather small: $Y \propto \rho^{0.4}$ (the change in the density between $0.9\rho_{W,bulk}$ of c-W films and $0.6\rho_{W,bulk}$ of a-W films would only account for 10%–15% change in Y), and cannot explain the significant difference between the erosion rates of c-W and a-W films. We therefore speculate that the latter is due to more complicated phenomena at the surface, which should be investigated in detail in the future. For example, due to the different oxygen and carbon concentration in the c-W and a-W films (Fig. 8), physical and chemical sputtering of these impurities could contribute to the different erosion behaviour of the samples. Thermal diffusion of oxygen embedded in the a-W films toward the surface [30] may also play a role. The topography cannot be invoked instead as a possible cause for the difference between the erosion rates of the samples since all the exposed films were characterised by a similar surface texture which consists of smooth peaks and valleys on the nanometre-scale, superimposed by a roughness having a RMS of few nanometres (see Table 2).

The dependence of the D+N plasma-W films interaction on the micro and nanostructure of the coatings is also evident from the XPS depth-profiling. For both the bias voltages, Fig. 9 clearly highlights that the nitrogen uptake of c-W films is higher than that of a-W films and the nitrogen profile of the former is also broader. We performed TRIM [38] simulations of nitrogen implantation into tungsten to interpret these results. We considered N^+ ions as projectiles. Contrary to N_2^+ ions, which divided into two nitrogen atoms with the same velocity when they reached the surface of the target, N^+ ions impinged with the full energy mainly determining the maximum nitrogen implantation depth. The total range of N^+ into tungsten, evaluated with TRIM, is ∼3 nm and ∼5 nm for ion energies of ∼120 eV and ∼320 eV. Before commenting the results of the simulations it is important to recall that TRIM describes the transport of energetic ions in matter on the basis of the binary collision approximation. It considers the target as fully amorphous (and therefore it is more suitable to study N implantation in a-W films than in c-W films) and it cannot describe the possible diffusion of thermalised species. For the a-W films, the total range at the two bias voltages seems to be in good agreement with the extent of the N profile as estimated by XPS depth-profiling (see Fig. 9). Considering the c-W films instead, the N profile extends further the total range at −300 V and goes far beyond at −100 V. Hence, we infer that atomic nitrogen diffusion sets on above 850 K for the a-W film and below 850 K for the c-W film. As a comparison, the study of the temperature dependence of N accumulation performed on PLANSEE polycrystalline tungsten samples [5] shows that nitrogen diffusion takes place above 800 K. The very low N diffusivity for a-W films could be due to their highly disordered structure as observed in [51] for hydrogen. Although Figs. 2, 3 and 10 show that these samples partially crystallised during the exposures, we conclude that their crystalline order remained sufficiently low to impede interstitial and grain boundary nitrogen diffusion. The fact that the morphological and structural changes endured by the a-W films did not significantly affect their interaction with nitrogen is supported by the results of other exposures to the D+N plasma of GyM reported in [9]. In that case, the lower sample temperature, plasma fluence and bias voltage considered did not modify the a-W films at the meso and nanoscale. However, the measured nitrogen retention was still lower than that of c-W films.

In the case of c-W films, it is interesting to note that the nitrogen profile of the sample exposed at −100 V goes more than twice deeper into the film than that of the sample exposed at −300 V. This could not only be explained by the longer exposure time for the experiment

at the lowest bias voltage (4 h instead of 3 h). Since the morphology and structure of the c-W films did not radically change after the two exposures (see Figs. 2 and 10), we argue that the corresponding different thickness of the N-enriched layer can be qualitatively understood in terms of the interplay between plasma sputtering (by both deuterium and nitrogen ions) and diffusion of nitrogen implanted in the films. It is reasonable to assume that the nitrogen profile in the c-W films goes like the ratio of the diffusivity to the sputtering velocity [52]. Being the temperature fixed at ~850 K, one may assume that the N diffusion coefficient is equal for the two exposures at −100 V and −300 V. Due to the energy dependence of the sputtering yield, the erosion velocity is instead clearly higher for the latter (see also Table 1). It follows that the ratio of the diffusivity to the sputtering velocity is lower at −300 V which, in turn, gives the thinner thickness where nitrogen was actually observed.

Regardless the very different properties of the films, a nitrogen-enriched surface layer was observed for every sample exposed to the D+N plasma of GyM, as highlighted by the XPS data of Section 3. This layer is thermally stable and does not decompose at least up to ~850 K. The present result is in agreement with [6] and [13]. Using the thermal desorption spectroscopy (TDS), the authors of [6] claim indeed that the main portion of retained nitrogen in different polycrystalline tungsten samples, exposed to a N seeded D plasma in the quantified plasma source PlaQ [53], was released as N_2 molecules around 1200 K under linear heating. TDS was also performed on WN_x films deposited by magnetron sputtering [13]. In [13], it was stated that the temperature at which the release of N_2 started was ~830 K but the TDS peaks were above 920 K.

Albeit the study of the deuterium retention of these films is out of the scope of the work, a comment can be made considering that all the samples were free of blisters after the experiments. This result was also reported in [9] for exposures at lower sample temperature, plasma fluence and bias voltage in GyM. The high temperature of our experiments goes into the direction of lowering the D retention of the films by defects recovery [54] (in case of a-W films the onset of the crystallisation process is evident from the SEM images of Figs. 2 and 3 and from the XRD spectra of Fig. 10). PLD W films on silicon with different morphology and structure, among which an a-W film and a columnar film having features very close to those of the MS c-W film considered in this work, were exposed to a pure deuterium plasma in GyM at a temperature of ~600 K, fluence of $6.7{\cdot}10^{24}$ ions·m^{-2} and bias voltage from 0 V to −300 V [31]. After the exposures, both the columnar and a-W films showed blisters with a typical dimension ranging between 40 μm and 170 μm, irrespective of the bias voltage, as a consequence of the accumulation of deuterium at the film–substrate interface. This high diffusivity of deuterium is mainly due to the contribution of grain boundaries which can be really important for nanocrystalline films [55].

Considering polycrystalline W bulk specimens, blisters were found after exposures in PlaQ [6,10] to: (i) a D plasma, (ii) a D plasma after a N plasma and (iii) a N seeded D plasma. Even if the exposure conditions are comparable with ours in terms of gas mixture, plasma flux and fluence, ion energy and sample temperature, the authors of [6] found that seeding the deuterium plasma with nitrogen resulted in an increase of the size of blisters in some cases. The sequential exposure to a nitrogen plasma and then to a deuterium plasma [10] at 500 K led to the formation of many large blisters with diameters up to ~ 40 μm on the surface of bulk polycrystalline W samples, while blisters were not detected without N pre-implantation. The authors claim that the W-N layer formed at 500 K could either act as a rather efficient diffusion barrier for D or could significantly reduce the recombination coefficient of D at the surface. The very different behaviour of bulk polycrystalline W samples and W films upon blister formation is related to their different crystallinity. Since blisters were not detected in both a-W and c-W specimens, the absence of blisters in W films is due to their nanocrystalline nature and not to a specific morphology and structure. Moreover, the role of nitrogen in hampering deuterium diffusion toward the substrate is evident by the fact that similar films exposed to a non-seeded deuterium plasma in GyM formed blisters [31]. In the case of the D+N plasma instead, we speculate that the implanted nitrogen was retained in interstitial sites, grain boundaries and defects decreasing deuterium diffusivity, especially the grain boundary diffusivity which is really important in the case of nanocrystalline films [55].

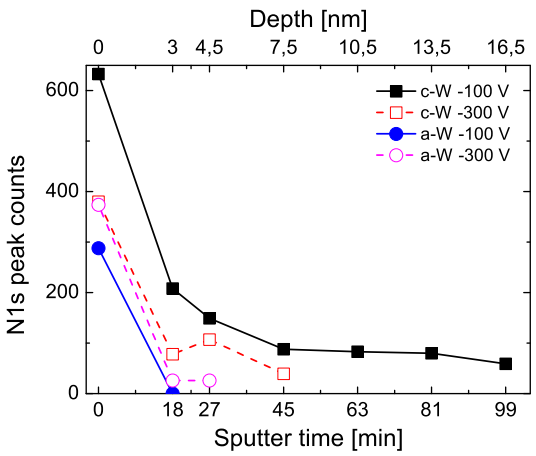

Fig. 9. N1s peak area as a function of the sputtering depth for the c-W (squares) and a-W (circles) films exposed at −100 V (full symbols and solid line) and at −300 V (open symbols and dashed line). Lines are drawn only to guide the eye. (For interpretation of the references to colour in this figure legend, the reader is referred to the web version of this article.)

5. Conclusions

Different nanostructured W films were exposed to a D+N plasma of the linear device GyM [20–22] at a temperature (~850 K), particle fluxes ($2 - 2.2 \times 10^{20}$ ions s^{-1} m^{-2}) and energies (up to ~320 eV) relevant to the main chamber of ITER [23] and the recessed regions of the DEMO first wall [24]. Magnetron sputtered columnar W (c-W) films and pulsed laser deposited amorphous W (a-W) films were considered in this study. On one side, c-W films can simulate the virgin W-coated tiles of JET-ILW and AUG [14]. On the other side, a-W films resemble nanostructured W-based deposits retrieved from present-day tokamaks and expected in ITER and DEMO [15,16,18,25]. Erosion, nitrogen uptake and compositional, morphological and structural modifications of c-W and a-W films induced by the D+N plasma of GyM were investigated via profilometry, X-ray depth-profiling photoelectron spectroscopy, optical microscopy, atomic force microscopy, scanning electron microscopy and X-ray diffraction measurements. Some conclusions can be schematically drawn from the results of the characterisation of the samples:

1. The erosion of a-W films is significantly lower than that of c-W films. The difference between the evaluated erosion rates cannot be explained neither by the different density of the coatings nor by topography-related effects and other more complicated surface phenomena should be invoked.
2. For all the films, a surface N-enriched layer, which is thermally stable and does not decompose, at least up to ~850 K, is observed.
3. Nitrogen uptake and diffusivity of c-W films are higher than those of a-W films. Nitrogen profile of a-W films extends to a depth comparable to the total ranges predicted by TRIM (which does not take into account thermal effects like diffusion) and goes instead beyond for c-W films. N diffusion sets on at a temperature above 850 K for the a-W film and below 850 K for

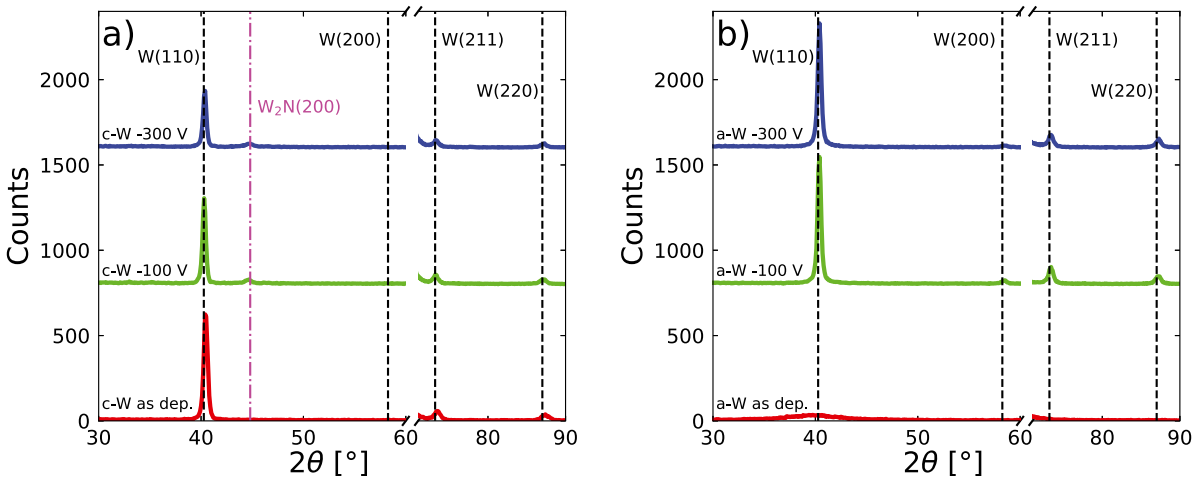

Fig. 10. XRD spectra of c-W (a) and a-W (b) films: as deposited (solid red line), exposed at −100 V (solid green line) and exposed at −300 V (solid blue line). The positions of the peaks of the α-phase of bulk W (dashed black lines) and the peak of $W_2N(200)$ (dash-dotted magenta line) are also indicated. A break from 60° to 71° was introduced to cut-off the strong Si(100) peak from the substrate. (For interpretation of the references to colour in this figure legend, the reader is referred to the web version of this article.)

the c-W film. The very low N diffusivity for a-W films could be due to their highly disordered structure as reported in [51] for hydrogen.

4. Contrary to what reported for polycrystalline W bulk samples [6, 10], both c-W and a-W films are free of blisters after the exposures. We infer that the different behaviour upon blister formation of W polycrystalline bulk specimens and nanostructured films is related to their different crystallinity. In particular, nitrogen retained in interstitial sites, grain boundaries and defects of c-W and a-W films may avoid the growth of deuterium blisters by reducing deuterium diffusivity paths.

From the point of view of the topic of plasma–wall interaction in tokamaks [3], these results give significant information related to the behaviour of W-coated tiles and amorphous W-based deposits exposed to a nitrogen seeded deuterium plasma with some ITER and DEMO relevant features. Once amorphous W deposits form on plasma facing components, they are hard to be eroded and quite inert to N. In particular, the very low N uptake of a-W films and their low N diffusivity indicate that the impinging nitrogen atoms and ions on W-based deposits would be mostly evacuated, giving a recycling factor for nitrogen close to 1. Since nitrogen retention in c-W films is higher and N diffusion sets on at a temperature below ~850 K, a lower value of the N recycling factor is expected for W-coated tiles. The information of recycling coefficient is highly desirable to improve the feedback control of the amount of the gas seeded into the plasma of tokamaks for radiative cooling.

After the exposures in GyM, the a-W deposits clearly changed at the meso and nanoscale, partially crystallising. However, they did not show any blister and sign of delamination. This has a twofold implication. First, no abrupt release of the retained N and D from a-W deposits as a consequence of blister bursting would take place during nitrogen seeded tokamak discharges. Second, a-W deposits would be well-adhered to the tokamak tiles and they thus would not flake, peel-off and form dust aggregates. These two statements can be safely extended to the c-W films. Moreover, contrary to the a-W specimens, they did not show any relevant morphological and structural modification thus witnessing the stability of tiles W coating toward D+N plasma exposure at high temperatures and ion energies.

CRediT authorship contribution statement

Andrea Uccello: Investigation, Writing - original draft, Writing - review & editing, Supervision. **Francesco Ghezzi:** Investigation, Writing - original draft, Writing - review & editing. **Laura Laguardia:** Investigation, Writing - original draft, Writing - review & editing. **Roberto Caniello:** Investigation. **David Dellasega:** Investigation, Resources, Writing - review & editing. **Fabio dell'Era:** Investigation. **Davide Della Torre:** Investigation. **Riccardo Donnini:** Investigation, Writing - review & editing. **Gustavo Granucci:** Investigation, Writing - review & editing. **Ernesto Mesto:** Investigation, Writing - review & editing. **Daniele Minelli:** Software, Investigation, Data curation. **Matteo Passoni:** Resources, Writing - review & editing. **Matteo Pedroni:** Investigation, Writing - review & editing. **Andrea Pezzoli:** Resources. **Daria Ricci:** Investigation, Writing - review & editing.

Declaration of competing interest

The authors declare that they have no known competing financial interests or personal relationships that could have appeared to influence the work reported in this paper.

Acknowledgements

The authors gratefully acknowledge IPP-Garching for providing the magnetron sputtered tungsten coatings. The authors also thank Dr. J. Kovac of Jožef Stefan Institute for useful discussions. This work has been carried out within the framework of the EUROfusion Consortium and has received funding from the Euratom research and training programme 2014–2018 and 2019–2020 under grant agreement No 633053. The views and opinions expressed herein do not necessarily reflect those of the European Commission. The activity has been performed under EUROfusion work-package plasma facing components (WP-PFC).

References

[1] A. Kallenbach, M. Bernert, R. Dux, L. Casali, T. Eich, L. Giannone, A. Herrmann, R. McDermott, A. Mlynek, H.W. Müller, F. Reimold, J. Schweinzer, M. Sertoli, G. Tardini, W. Treutterer, E. Viezzer, R. Wenninger, M. Wischmeier, the ASDEX Upgrade Team, Impurity seeding for tokamak power exhaust: from present devices via ITER to DEMO, Plasma Phys. Control. Fusion 55 (12) (2013) 124041.

[2] A. Kallenbach, M. Balden, R. Dux, T. Eich, C. Giroud, A. Huber, G.P. Maddison, M. Mayer, K. McCormick, R. Neu, T.W. Petrie, T. Pütterich, J. Rapp, M.L. Reinke, K. Schmid, J. Schweinzer, S. Wolfe, Plasma surface interactions in impurity seeded plasmas, J. Nuclear Mater. 415 (1) (2011) S19 – S26, Proceedings of the 19th International Conference on Plasma-Surface Interactions in Controlled Fusion.

[3] S. Brezinsek, J.W. Coenen, T. Schwarz-Selinger, K. Schmid, A. Kirschner, A. Hakola, F.L. Tabares, H.J. van der Meiden, M.L. Mayoral, M. Reinhart, E. Tsitrone, T. Ahlgren, M. Aints, M. Airila, S. Almaviva, E. Alves, T. Angot, V. Anita, R. Arredondo Parra, F. Aumayr, M. Balden, J. Bauer, M. Ben Yaala, B.M. Berger, R. Bisson, C. Björkas, I. Bogdanovic Radovic, D. Borodin, J. Bucalossi, J. Butikova, B. Butoi, I. Čadež, R. Caniello, L. Caneve, G. Cartry, N. Catarino, M. Čekada, G. Ciraolo, L. Ciupinski, F. Colao, Y. Corre, C. Costin, T. Craciunescu, A. Cremona, M. De Angeli, A. de Castro, R. Dejarnac, D. Dellasega, P. Dinca, T. Dittmar, C. Dobrea, P. Hansen, A. Drenik, T. Eich, S. Elgeti, D. Falie, N. Fedorczak, Y. Ferro, T. Fornal, E. Fortuna-Zalesna, L. Gao, P. Gasior, M. Gherendi, F. Ghezzi, Ž. Gosar, H. Greuner, E. Grigore, C. Grisolia, M. Groth, M. Gruca, J. Grzonka, J.P. Gunn, K. Hassouni, K. Heinola, T. Höschen, S. Huber, W. Jacob, I. Jepu, X. Jiang, I. Jogi, A. Kaiser, J. Karhunen, M. Kelemen, M. Köppen, H.R. Koslowski, A. Kreter, M. Kubkowska, M. Laan, L. Laguardia, A. Lahtinen, A. Lasa, V. Lazic, N. Lemahieu, J. Likonen, J. Linke, A. Litnovsky, C. Linsmeier, T. Loewenhoff, C. Lungu, M. Lungu, G. Maddaluno, H. Maier, T. Makkonen, A. Manhard, Y. Marandet, S. Markelj, L. Marot, C. Martin, A.B. Martin-Rojo, Y. Martynova, R. Mateus, D. Matveev, M. Mayer, G. Meisl, N. Mellet, A. Michau, J. Miettunen, S. Möller, T.W. Morgan, J. Mougenot, M. Mozetič, V. Nemanič, R. Neu, K. Nordlund, M. Oberkofler, E. Oyarzabal, M. Panjan, C. Pardanaud, P. Paris, M. Passoni, B. Pegourie, P. Pelicon, P. Petersson, K. Piip, G. Pintsuk, G.O. Pompilian, G. Popa, C. Porosnicu, G. Primc, M. Probst, J. Räisänen, M. Rasinski, S. Ratynskaia, D. Reiser, D. Ricci, M. Richou, J. Riesch, G. Riva, M. Rosinski, P. Roubin, M. Rubel, C. Ruset, E. Safi, G. Sergienko, Z. Siketic, A. Sima, B. Spilker, R. Stadlmayr, I. Steudel, P. Ström, T. Tadic, D. Tafalla, I. Tale, D. Terentyev, A. Terra, V. Tiron, I. Tiseanu, P. Tolias, D. Tskhakaya, A. Uccello, B. Unterberg, I. Uytdenhoven, E. Vassallo, P. Vavpetič, P. Veis, I.L. Velicu, J.W.M. Vernimmen, A. Voitkans, U. von Toussaint, A. Weckmann, M. Wirtz, A. Založnik, R. Zaplotnik, WP PFC contributors, Plasma–wall interaction studies within the EUROfusion consortium: progress on plasma-facing components development and qualification, Nucl. Fusion 57 (11) (2017) 116041.

[4] K. Schmid, A. Manhard, C. Linsmeier, A. Wiltner, T. Schwarz-Selinger, W. Jacob, S. Mändl, Interaction of nitrogen plasmas with tungsten, Nucl. Fusion 50 (2) (2010) 025006.

[5] G. Meisl, K. Schmid, O. Encke, T. Höschen, L. Gao, C. Linsmeier, Implantation and erosion of nitrogen in tungsten, New J. Phys. 16 (9) (2014) 093018.

[6] O.V. Ogorodnikova, K. Sugiyama, A. Markin, Y. Gasparyan, V. Efimov, A. Manhard, M. Balden, Effect of nitrogen seeding into deuterium plasma on deuterium retention in tungsten, Phys. Scr. 2011 (T145) (2011) 014034.

[7] H.T. Lee, M. Ishida, Y. Ohtsuka, Y. Ueda, The influence of nitrogen on deuterium permeation through tungsten, Phys. Scr. 2014 (T159) (2014) 014021.

[8] H.T. Lee, G. De Temmerman, L. Gao, T. Schwarz-Selinger, G. Meisl, T. Höschen, Y. Ueda, Deuterium retention in tungsten exposed to mixed D+N plasma at divertor relevant fluxes in Magnum-PSI, J. Nuclear Mater. 463 (2015) 974–978, PLASMA-SURFACE INTERACTIONS 21.

[9] L. Laguardia, R. Caniello, A. Cremona, D. Dellasega, F. Dell'Era, F. Ghezzi, G. Gittini, G. Granucci, V. Mellera, D. Minelli, F. Pallotta, M. Passoni, D. Ricci, E. Vassallo, Ammonia formation and W coatings interaction with deuterium/nitrogen plasmas in the linear device GyM, J. Nuclear Mater. 463 (2015) 680–683, PLASMA-SURFACE INTERACTIONS 21.

[10] L. Gao, W. Jacob, P. Wang, U. von Toussaint, A. Manhard, Influence of nitrogen pre-implantation on deuterium retention in tungsten, Phys. Scr. 2014 (T159) (2014) 014023.

[11] L. Gao, W. Jacob, T. Schwarz-Selinger, A. Manhard, Deuterium implantation into tungsten nitride: Negligible diffusion at 300 K, J. Nuclear Mater. 451 (1) (2014) 352–355.

[12] E. Vassallo, R. Caniello, G. Angella, D. Dellasega, G. Granucci, V. Mellera, D. Minelli, M. Pedroni, D. Ricci, V. Rigato, M. Passoni, Retention of nanocrystalline WN_x layers exposed to high-fluence deuterium plasmas, J. Nuclear Mater. 466 (2015) 621–626.

[13] L. Gao, W. Jacob, G. Meisl, T. Schwarz-Selinger, T. Höschen, U. von Toussaint, T. Dürbeck, Interaction of deuterium plasma with sputter-deposited tungsten nitride films, Nucl. Fusion 56 (1) (2016) 016004.

[14] C. Ruset, E. Grigore, H. Maier, R. Neu, H. Greuner, M. Mayer, G. Matthews, Development of W coatings for fusion applications, Fusion Eng. Des. 86 (9) (2011) 1677–1680, Proceedings of the 26th Symposium of Fusion Technology (SOFT-26).

[15] M. Rasinski, E. Fortuna-Zalesna, M. Mayer, R. Neu, T. Plocinski, M. Lewandowska, K.J. Kurzydlowski, the ASDEX Upgrade Team, High resolution scanning transmission electron microscopy (HR STEM) analysis of re-deposited layer on ASDEX Upgrade tile, Fusion Eng. Des. 86 (9) (2011) 1753–1756, Proceedings of the 26th Symposium of Fusion Technology (SOFT-26).

[16] A. Litnovsky, M. Matveeva, A. Herrmann, V. Rohde, M. Mayer, K. Sugiyama, K. Krieger, V. Voitsenya, G. Vayakis, A.E. Costley, R. Reichle, G.D. Temmerman, S. Richter, U. Breuer, L. Buzi, S. Müller, V. Philipps, U. Samm, P. Wienhold, the ASDEX Upgrade Team, First studies of ITER-diagnostic mirrors in a tokamak with an all-metal interior: results of the first mirror test in ASDEX Upgrade, Nucl. Fusion 53 (7) (2013) 073033.

[17] A. Baron-Wiechec, E. Fortuna-Zaleśna, J. Grzonka, M. Rubel, A. Widdowson, C. Ayres, J.P. Coad, C. Hardie, K. Heinola, G.F. Matthews, the JET Contributors, First dust study in JET with the ITER-like wall: sampling, analysis and classification, Nucl. Fusion 55 (11) (2015) 113033.

[18] E. Fortuna-Zalesna, M. Andrzejczuk, L. Ciupinski, K. Rozniatowski, K. Sugiyama, M. Mayer, K.J. Kurzydlowski, the ASDEX Upgrade Team, Post mortem analysis of a tungsten coated tile from the outer divertor strike point region of ASDEX upgrade, Nuclear Mater. Energy 9 (2016) 128–131.

[19] E. Fortuna-Zaleśna, J. Grzonka, M. Rubel, A. Garcia-Carrasco, A. Widdowson, A. Baron-Wiechec, L. Ciupiński, the JET Contributors, Studies of dust from JET with the ITER-Like Wall: Composition and internal structure, Nuclear Mater. Energy 12 (2017) 582–587, Proceedings of the 22nd International Conference on Plasma Surface Interactions 2016, 22nd PSI.

[20] G. Granucci, D. Ricci, S. Alocci, B. Baiocchi, W. Bin, A. Bruschi, A. Cremona, O. D'Arcangelo, M. De Angeli, F. Dell'Era, F. Gandini, S. Garavaglia, G. Gatto, G. Gervasini, G. Gittini, G. Grossetti, G. Grosso, E. Lazzaro, M. Lontano, V. Mellera, V. Muzzini, A. Moro, A. Nardone, R. Schiavone, N. Spinicchia, C. Sozzi, The new linear plasma device GyM at IFP-CNR, in: Proceeding of the 36th EPS Conference, Vol. 33E, June 29–July 3 2009, Sofia, Bulgaria, ECA, 2009, P-4.148.

[21] D. Ricci, D. Iraji, A. Cremona, I. Furno, S. Garavaglia, G. Granucci, M. Lontano, V. Mellera, D. Minelli, Experimental characterization of instabilities in the linear machine GyM, in: Proceeding of the 39th EPS Conference, Vol. 36F, 26 July 2012, Stockholm, Sweden, ECA, 2012, P-4.164.

[22] M. Sala, E. Tonello, A. Uccello, X. Bonnin, D. Ricci, D. Dellasega, G. Granucci, M. Passoni, Simulations of Argon plasmas in the linear plasma device GyM with the SOLPS-ITER code, Plasma Phys. Control. Fusion 62 (5) (2020) 055005.

[23] G. Federici, J.N. Brooks, D.P. Coster, G. Janeschitz, A. Kukuskhin, A. Loarte, H.D. Pacher, J. Stober, C.H. Wu, Assessment of erosion and tritium codeposition in ITER-FEAT, J. Nuclear Mater. 290 (Suppl. C) (2001) 260–265, 14th Int. Conf. on Plasma-Surface Interactions in Controlled Fusion Devices.

[24] J. Roth, K. Sugiyama, V. Alimov, T. Höschen, M. Baldwin, R. Doerner, EUROFER as wall material: Reduced sputtering yields due to W surface enrichment, J. Nuclear Mater. 454 (1) (2014) 1–6.

[25] A. Maffini, A. Uccello, D. Dellasega, M. Passoni, Laser cleaning of diagnostic mirrors from tungsten-oxygen tokamak-like contaminants, Nucl. Fusion 56 (8) (2016) 086008.

[26] P. Wang, W. Jacob, L. Gao, S. Elgeti (Lindig), M. Balden, Deuterium retention in tungsten films deposited by magnetron sputtering, Phys. Scr. 2014 (T159) (2014) 014046.

[27] R. Caniello, A. Uccello, F. Ghezzi, D. Minelli, I. Bogdanović Radović, Z. Siketić, A. Cremona, F. Dell'Era, G. Gittini, V. Mellera, F. Pallotta, M. Pedroni, D. Ricci, N. Spinicchia, E. Vassallo, Erosion yield and W surface enrichment of Fe-W model system exposed to low flux deuterium plasma in the linear device GyM, Nuclear Mater. Energy 10 (2017) 9–16.

[28] K. Sugiyama, K. Schmid, W. Jacob, Sputtering of iron, chromium and tungsten by energetic deuterium ion bombardment, Nuclear Mater. Energy 8 (Suppl. C) (2016) 1–7.

[29] D. Dellasega, G. Merlo, C. Conti, C.E. Bottani, M. Passoni, Nanostructured and amorphous-like tungsten films grown by pulsed laser deposition, J. Appl. Phys. 112 (8) (2012) 084328.

[30] D. Dellasega, S.M. Pietralunga, A. Pezzoli, V. Russo, L. Nasi, C. Conti, M.J. Vahid, A. Tagliaferri, M. Passoni, Tungsten oxide nanowires grown on amorphous-like tungsten films, Nanotechnology 26 (36) (2015) 365601.

[31] M. Sala, A. Uccello, D. Dellasega, M. Pedroni, E. Vassallo, M. Passoni, Exposures of bulk W and nanostructured W coatings to medium flux D plasmas, Nuclear Mater. Energy 24 (2020) 100779.

[32] W. Eckstein, C. García-Rosales, J. Roth, W. Ottenberger, Sputtering Data, IPP Report 9/82, Max-Planck-Institut für Plasmaphysik, Garching, 1993, http://hdl.handle.net/11858/00-001M-0000-0027-6324-6.

[33] N. Matsunami, Y. Yamamura, Y. Itikawa, N. Itoh, Y. Kazumata, S. Miyagawa, K. Morita, R. Shimizu, H. Tawara, Energy dependence of the ion-induced sputtering yields of monatomic solids, At. Data Nucl. Data Tables 31 (1) (1984) 1–80.

[34] F. Ghezzi, L. Laguardia, R. Caniello, A. Canton, S. Dal Bello, B. Rais, M. Anderle, XPS, SIMS and FTIR-ATR characterization of boronized graphite from the thermonuclear plasma device RFX-mod, Appl. Surf. Sci. 354 (2015) 408–419, European Conference on Surface Science 2014.

[35] Y.M. Cross, J.E. Castle, The relationship between transmission efficiencies in the FRR and fat modes of an electron spectrometer, J. Electron Spectrosc. Relat. Phenom. 22 (1) (1981) 53–60.

[36] J.J. Yeh, I. Lindau, Atomic subshell photoionization cross sections and asymmetry parameters: $1 \leq Z \leq 103$, At. Data Nucl. Data Tables 32 (1) (1985) 1–155.

[37] P. Ruffieux, P. Schwaller, O. Gröning, L. Schlapbach, P. Gröning, Q.C. Herd, D. Funnemann, J. Westermann, Experimental determination of the transmission factor for the Omicron EA125 electron analyzer, Rev. Sci. Instrum. 71 (10) (2000) 3634–3639.

[38] J. Biersack, Computer simulations of sputtering, Nuclear Inst. Methods Phys. Res. B 27 (1) (1987) 21–36.

[39] D. Nečas, P. Klapetek, Gwyddion: an open-source software for SPM data analysis, Central Eur. J. Phys. 10 (2012) 181–188.

[40] C.C. Baker, S. Ismat Shah, Reactive sputter deposition of tungsten nitride thin films, J. Vac. Sci. Technol. A 20 (5) (2002) 1699–1703.
[41] G. Soto, W. de la Cruz, F.F. Castillón, J.A. Díaz, R. Machorro, M.H. Farías, Tungsten nitride films grown via pulsed laser deposition studied in situ by electron spectroscopies, Appl. Surf. Sci. 214 (2003) 58–67.
[42] Z. Wang, Z. Liu, Z. Yang, S. Shingubara, Characterization of sputtered tungsten nitride film and its application to Cu electroless plating, Microelectron. Eng. 85 (2) (2008) 395–400.
[43] L. Johansson, Electronic and structural properties of transition-metal carbide and nitride surfaces, Surf. Sci. Rep. 21 (5–6) (1995) 177–250.
[44] J. Kovac, Josef Stefan Institute, 2017-05-08, private communication.
[45] I. Tajima, M. Yamamoto, Characterization of plasma polymers from tetramethylsilane, octamethylcyclotetrasiloxane, and methyltrimethoxysilane, J. Polym. Sci. A 25 (7) (1987) 1737–1744.
[46] H. Kiyooka, O. Matsumoto, Reaction scheme of ammonia synthesis in the ECR plasmas, Plasma Chem. Plasma Process. 16 (4) (1996) 547–562.
[47] M. Ben Yaala, L. Marot, R. Steiner, L. Moser, G. De Temmerman, C. Porosnicu, C.P. Lungu, M. Oberkofler, E. Meyer, Quartz micro-balance and in situ XPS study of the adsorption and decomposition of ammonia on gold, tungsten, boron, beryllium and stainless steel surfaces, Nucl. Fusion 58 (10) (2018) 106012.
[48] Y.-M. Sun, E.R. Engbrecht, T. Bolom, C. Cilino, J.H. Sim, J.M. White, J.G. Ekerdt, K. Pfeifer, Ultra thin tungsten nitride film growth on dielectric surfaces, Thin Solid Films 458 (1) (2004) 251–256.
[49] A.L. Patterson, The Scherrer formula for X-ray particle size determination, Phys. Rev. 56 (10) (1939) 978.
[50] V.I. Shulga, The density and binding effects in sputtering by ions of widely varying masses, Nucl. Instrum. Methods Phys. Res. B 195 (3) (2002) 291–301.
[51] V. Nemanič, B. Zajec, D. Dellasega, M. Passoni, Hydrogen permeation through disordered nanostructured tungsten films, J. Nuclear Mater. 429 (1) (2012) 92–98.
[52] P.S. Ho, Effects of enhanced diffusion on preferred sputtering of homogeneous alloy surfaces, Surf. Sci. 72 (2) (1978) 253–263.
[53] O.V. Ogorodnikova, T. Schwarz-Selinger, K. Sugiyama, T. Dürbeck, W. Jacob, Deuterium retention in different tungsten grades, Phys. Scr. (T138) (2009) 014053.
[54] M.J. Simmonds, Y.Q. Wang, J.L. Barton, M.J. Baldwin, J.H. Yu, R.P. Doerner, G.R. Tynan, Reduced deuterium retention in simultaneously damaged and annealed tungsten, J. Nuclear Mater. 494 (2017) 67–71.
[55] J.D. Fast, Gases in Metals, Macmillan International Higher Education, 2016.